The Implementation of Magnetic Islands in Gyrokinetic Toroidal Code*

JIANG Peng (江澎)[1,2], LIN Zhihong (林志宏)[2], Ihor HOLOD[2],
XIAO Chijie (肖池阶)[1]

[1]Fusion Simulation Center and State Key Laboratory of Nuclear Physics and Technology, Peking University, Beijing 100871, China
[2]Department of Physics and Astronomy, University of California, Irvine, California 92697, USA

Abstract The implementation of magnetic islands in gyrokinetic simulation has been verified in the gyrokinetic toroidal code (GTC). The ion and electron density profiles become partially flattened inside the islands. The density profile at the low field side is less flattened than that at the high field side due to toroidally trapped particles in the low field side, which do not move along the perturbed magnetic field lines. When the fraction of trapped particles decreases, the density profile at the low field becomes more flattened.

Keywords: magnetic islands, toroidal plasma confinement, plasma gyrokinetics, magnetic fields

PACS: *52.30.Gz, 52.55.Fa, 52.65.Tt*

DOI: 10.1088/1009-0630/18/2/05

(Some figures may appear in colour only in the online journal)

1 Introduction

In fusion experiments, axisymmetric magnetic fields form nested surfaces to confine charged particles in toroidal geometry. However, the topology of the magnetic surfaces can be destroyed by external perturbation or magnetic reconnection which creates magnetic islands. The plasma pressure profile flattening across the islands reduces the local bootstrap current and gives rise to a nonlinear tearing instability, namely the neoclassical tearing mode (NTM) [1]. The NTM, which has been observed in tokamak experiments [2], can produce large islands and limit the performance of a fusion reactor. Therefore, the NTM can be a big threat to the H-mode operation in ITER (International Thermonuclear Experimental Reactor) [3].

The NTM prediction currently relies on empirical scaling or reduced theoretical models [4]. A popular dynamical model for the island growth uses a modified Rutherford equation [5] together with some analytic formulation of the instability drive of various current channels including bootstrap current and polarization current [6]. Direct numerical simulation is needed for better understanding and eventual real time control of tokamak plasma turbulence [7]. First-principles NTM simulation remains a computational grand challenge due to the nonlinear interaction between multiple physical processes covering disparate spatial-temporal scales.

As the first step toward building the capability for first-principles NTM simulation, we limit the current simulation to the dynamical time scale of microturbulence. Because the island evolution time is much longer than the time scale of microturbulence, the magnetic islands are assumed to be static during the microturbulence simulations. The nonlinear interaction between static magnetic islands and microturbulence has been studied recently [8−12]. The response of the particle motion to the islands can be complicated in the toroidal geometry. For example, the trajectories of test particles may deviate from the perturbed field lines induced by the magnetic islands [8]. The density and temperature profiles inside the islands can be flattened more significantly in the high field side than in the low field side because of the toroidally trapped particles [13].

In this paper, we formulate and verify the gyrokinetic simulation with static islands. Global particle simulation has been used to study the effects of the static magnetic islands in toroidal geometry [14]. Our simulations find that the ion and electron density profiles become partially flattened inside the islands. The density profile at the low field side is less flattened than that at the high field side because there are more toroidally trapped particles on the low field side, which do not move along the perturbed magnetic field lines. When the fraction of trapped particles decreases, the density profile at the low field becomes more flattened. Our work utilizes the particle-in-cell gyrokinetic toroidal

*supported by National Special Research Program of China for ITER (Nos. 2013GB111000 and 2014GB107004), China Scholarship Council (No. 2011601098), U.S. DOE Grants DE-SC0010416 and DE-FG02-07ER54916

code (GTC) [15−17], which has been extensively applied to study neoclassical transport [18], energetic particle transport [19], ion and electron temperature gradient modes [20,21], collisionless trapped electron mode [22], Alfvèn eigenmodes [23,24], kink modes [25] and tearing modes [26]. Electrostatic simulations of the island effects on the ITG with adiabatic electrons have been studied [14]. The capabilities will provide the first-principles tool for self-consistent simulation of NTM including the interactions between neoclassical transport, microturbulence and MHD stability.

This paper is organized as follows. In section 2, we first describe the implementation of magnetic islands in the toroidal geometry, and derive the gyrokinetic equations of motion in the presence of static islands. In section 3, the island implementation is verified and the effects of static islands on density profiles are discussed. Finally, the conclusions are in section 4.

2 Simulation formulation

In our simulations, the toroidal magnetic coordinate system (ψ, θ, ζ) is used where ψ is the poloidal magnetic flux function, θ is the magnetic poloidal angle, and ζ is the magnetic toroidal angle. The covariant representation of the magnetic field [27] is

$$\mathbf{B}_0 = \delta\nabla\psi + I\nabla\theta + g\nabla\zeta, \tag{1}$$

the contravariant representation is

$$\mathbf{B}_0 = q\nabla\psi \times \nabla\theta - \nabla\psi \times \nabla\zeta, \tag{2}$$

and the Jacobian is

$$J^{-1} = \nabla\psi \cdot \nabla\theta \times \nabla\zeta = \frac{B_0^2}{gq + I}. \tag{3}$$

The radial component $\delta\nabla\psi$ is small and usually neglected [27]. The island is introduced through a perturbed vector potential parallel to the background magnetic field,

$$\mathbf{A}_\mathrm{I} = \alpha\mathbf{B}_0, \tag{4}$$

where $\alpha = \alpha_0(\psi)\cos(m\theta - n\zeta)$. We neglect the equilibrium current in this work, i.e. $\nabla \times \mathbf{B}_0 = 0$, so the island magnetic field perturbation is

$$\begin{aligned}\delta\mathbf{B}_\mathrm{I} &= \nabla\alpha \times \mathbf{B}_0 \\ &= \frac{\partial\alpha}{\partial\psi} I\nabla\psi \times \nabla\theta + \frac{\partial\alpha}{\partial\psi} g\nabla\psi \times \nabla\zeta \\ &\quad + \left(\frac{\partial\alpha}{\partial\zeta} I - \frac{\partial\alpha}{\partial\theta} g\right)\nabla\zeta \times \nabla\theta.\end{aligned} \tag{5}$$

In the current work, we only consider the effects of magnetic field induced by the islands. The neoclassical effects have been included in an ongoing study of island effects on bootstrap current. Since the nested magnetic surfaces are destroyed by the island, the poloidal magnetic flux function ψ is no longer valid. A new helical flux function ψ_he [28] satisfies the constraint condition $(\mathbf{B}_0 + \delta\mathbf{B}_\mathrm{I}) \cdot \nabla\psi_\mathrm{he} = 0$. The helical flux function can be represented as

$$\psi_\mathrm{he} = \psi - \frac{\psi_\mathrm{t}}{q_\mathrm{s}} - \alpha_0 g\cos m\xi, \tag{6}$$

where $\xi = \theta - \zeta/q_\mathrm{s}$, q_s is the safety factor of the resonant surface and ψ_t is a toroidal flux function on the resonant surface. The total magnetic field with island perturbation is

$$\mathbf{B} = q\nabla\psi \times \nabla\xi - \nabla\psi_\mathrm{he} \times \nabla\zeta. \tag{7}$$

It is obvious that the constraint condition $\mathbf{B}\cdot\nabla\psi_\mathrm{he} = 0$ is satisfied. We define the island width W as the distance from island center to island separatrix at $\theta = 0$, which can be represented as

$$W = \sqrt{\frac{4R_0^2\alpha_0 q_\mathrm{s}}{\mathrm{d}q_\mathrm{s}/\mathrm{d}r}}\ , \tag{8}$$

where $\mathrm{d}q_\mathrm{s}/\mathrm{d}r$ is the gradient of the q profile at the resonant surface and R_0 is the major radius.

The gyrokinetic equation with island perturbation, using the gyrocenter position $\mathbf{X}$, magnetic moment μ, and the parallel velocity $v_\parallel$ as a set of independent variables, reads,

$$\frac{\mathrm{d}}{\mathrm{d}t} f_j = \left[\frac{\partial}{\partial t} + \dot{\mathbf{X}}\cdot\nabla + \dot{v_\parallel}\frac{\partial}{\partial v_\parallel}\right] f_j = 0, \tag{9}$$

$$\dot{\mathbf{X}} = v_\parallel \frac{\mathbf{B}}{B_0} + \mathbf{v}_E + \mathbf{v}_\mathrm{d}, \tag{10}$$

$$\dot{v_\parallel} = -\frac{1}{m_j}\frac{\mathbf{B}^*}{B_0}\left(\mu\nabla B_0 + Z_j\nabla\phi\right), \tag{11}$$

where index $j =$ i, e stands for ion or electron, while Z_j and m_j are the particle charge and mass, respectively. The equilibrium magnetic field is much larger than the island magnetic field, $B_0 \gg \delta B_\mathrm{I}$, so we treat the island magnetic field as a perturbation in the gyrokinetic equation. $\mathbf{B}_0 = B_0\mathbf{b}_0$ is the equilibrium magnetic field, $\mathbf{B} = \mathbf{B}_0 + \delta\mathbf{B}_\mathrm{I}$, and

$$\mathbf{B}^* = \mathbf{B}_0^* + \delta\mathbf{B}_\mathrm{I} = \mathbf{B}_0 + \frac{B_0 v_\parallel}{\Omega_j}\nabla\times\mathbf{b}_0 + \delta\mathbf{B}_\mathrm{I}. \tag{12}$$

The $\mathbf{E}\times\mathbf{B}$ drift velocity is

$$\mathbf{v}_E = \frac{c\mathbf{b}_0\times\nabla\phi}{B_0}, \tag{13}$$

and the magnetic drift velocity is

$$\mathbf{v}_\mathrm{d} = \mathbf{v}_\mathrm{c} + \mathbf{v}_\mathrm{g}, \tag{14}$$

where the magnetic curvature drift is

$$\mathbf{v}_\mathrm{c} = \frac{v_\parallel^2}{\Omega_j}\nabla\times\mathbf{b}_0, \tag{15}$$

and the grad-B drift is

$$\mathbf{v}_\mathrm{g} = \frac{\mu}{m_j\Omega_j}\mathbf{b}_0\times\nabla B_0. \tag{16}$$

The electrostatic potential can be found using a gyrokinetic Poisson equation, assuming a single ion species,

$$\frac{4\pi Z_{\rm i}^2 n_{\rm i}}{T_{\rm i}}\left(\phi-\tilde{\phi}\right)=4\pi\left(Z_{\rm i}n_{\rm i}-en_{\rm e}\right). \tag{17}$$

The density is defined as the fluid moments of the corresponding distribution function,

$$n=\int f{\rm d}\mathbf{v}, \tag{18}$$

where

$$\int {\rm d}\mathbf{v}\equiv\frac{\pi B_0}{m}\int {\rm d}v_\parallel {\rm d}\mu. \tag{19}$$

The distribution function can be decomposed into equilibrium and perturbed parts $f=f_0+\delta f$. The equilibrium part satisfies the gyrokinetic equation,

$$\frac{\partial}{\partial t}f_{0j}+\left(v_\parallel\mathbf{b}_0+\mathbf{v}_{\rm d}\right)\cdot\nabla f_{0j}-\frac{\mu}{m_j}\frac{\mathbf{B}_0^*}{B_0}\cdot\nabla B_0\frac{\partial}{\partial v_\parallel}f_{0j}=0. \tag{20}$$

Subtracting Eq. (20) from Eq. (9) and defining the particle weight as $w_j=\frac{\delta f_j}{f_j}$, the weight equation for ions and electrons with island perturbation can be rewritten as

$$\begin{aligned}\frac{{\rm d}w_j}{{\rm d}t}=&(1-w_j)\Big[-\left(v_\parallel\frac{\delta\mathbf{B}_{\rm I}}{B_0}+\mathbf{v}_E\right)\cdot\frac{\nabla f_{0j}}{f_{0j}}\\&+\left(\mu\frac{\delta\mathbf{B}_{\rm I}}{B_0}\cdot\nabla B_0+Z_j\frac{\mathbf{B}^*}{B_0}\cdot\nabla\phi\right)\frac{1}{m_j f_{0j}}\frac{\partial f_{0j}}{\partial v_\parallel}\Big],\end{aligned} \tag{21}$$

where the operator ${\rm d}/{\rm d}t$ on the left hand side is defined by Eqs. (9), (10) and (11), and the magnetic flutter term on the right hand side of Eq. (21) is the main contribution of island perturbation.

When we add magnetic islands to the tokamak equilibrium, we continue to use the equilibrium grids, i.e., the same grids as those used in the equilibrium with unperturbed, closed flux surfaces. So we can still locate the grids using the unperturbed flux surfaces.

Assuming the radial derivatives of g and I to be zero, the guiding center equations of motion [27] with island perturbation are

$$\dot{\zeta}=\frac{v_\parallel B_0\left(q+I\partial_\psi\alpha\right)}{D}-c\frac{I}{D}\left(\frac{\partial\phi}{\partial\psi}+\frac{1}{Z_j}\frac{\partial\varepsilon}{\partial B_0}\frac{\partial B_0}{\partial\psi}\right), \tag{22}$$

$$\dot{\theta}=\frac{v_\parallel B_0\left(1-g\partial_\psi\alpha\right)}{D}+c\frac{g}{D}\left(\frac{\partial\phi}{\partial\psi}+\frac{1}{Z_j}\frac{\partial\varepsilon}{\partial B_0}\frac{\partial B_0}{\partial\psi}\right), \tag{23}$$

$$\begin{aligned}\dot{\psi}=&v_\parallel B_0\left(\frac{g}{D}\frac{\partial\alpha}{\partial\theta}-\frac{I}{D}\frac{\partial\alpha}{\partial\zeta}\right)+c\frac{I}{D}\left(\frac{\partial\phi}{\partial\zeta}+\frac{1}{Z_j}\frac{\partial\varepsilon}{\partial B_0}\frac{\partial B_0}{\partial\zeta}\right)\\&-c\frac{g}{D}\left(\frac{\partial\phi}{\partial\theta}+\frac{1}{Z_j}\frac{\partial\varepsilon}{\partial B_0}\frac{\partial B_0}{\partial\theta}\right),\end{aligned} \tag{24}$$

$$\begin{aligned}\dot{\rho_\parallel}=&-c\frac{\left(1-g\partial_\psi\alpha\right)}{D}\left(\frac{\partial\phi}{\partial\theta}+\frac{1}{Z_j}\frac{\partial\varepsilon}{\partial B_0}\frac{\partial B_0}{\partial\theta}\right)\\&-c\frac{\left(q+I\partial_\psi\alpha\right)}{D}\left(\frac{\partial\phi}{\partial\zeta}+\frac{1}{Z_j}\frac{\partial\varepsilon}{\partial B_0}\frac{\partial B_0}{\partial\zeta}\right)\\&+c\frac{\left(I\partial_\zeta\alpha-g\partial_\theta\alpha\right)}{D}\left(\frac{\partial\phi}{\partial\psi}+\frac{1}{Z_j}\frac{\partial\varepsilon}{\partial B_0}\frac{\partial B_0}{\partial\psi}\right),\end{aligned} \tag{25}$$

where $D=gq+I$ and $\frac{\partial\varepsilon}{\partial B_0}=\mu+\frac{Z_j^2}{m_jc^2}\rho_\parallel^2B_0$. The modified parallel canonical momentum is $\rho_{\rm c}=\rho_\parallel+\alpha$ with $\rho_\parallel=\frac{v_\parallel}{\Omega_j}=\frac{m_jc}{Z_jB_0}v_\parallel$.

Assuming a Maxwellian distribution for the parallel and perpendicular velocity, the gyrokinetic weight equation for ions and electrons with island perturbation can be rewritten as

$$\begin{aligned}\frac{{\rm d}w_j}{{\rm d}t}=&(1-w_j)\Big[-\left(\frac{c}{B_0}\mathbf{b}_0\times\nabla\phi+v_\parallel\frac{\delta\mathbf{B}_{\rm I}}{B_0}\right)\cdot\left.\frac{\nabla f_0}{f_0}\right|_{v_\perp}\\&-\frac{Z_j}{T_j}\left(v_\parallel\mathbf{b}_0+v_\parallel\frac{\delta\mathbf{B}_{\rm I}}{B_0}+\mathbf{v}_{\rm d}\right)\cdot\nabla\phi\Big].\end{aligned} \tag{26}$$

Here, we take derivatives at $v_\perp=$ const instead of $\mu=$ const. If we assume that α is independent of ψ, i.e. $\frac{\partial\alpha}{\partial\psi}=0$ and ignore the equilibrium current I, only the radial component is left in Eq. (5). Assuming the background density and temperature being radial ψ dependent only and considering only the radial component of the island perturbed magnetic field, the weight equation with island perturbation in Boozer coordinates is

$$\begin{aligned}\frac{{\rm d}w_j}{{\rm d}t}=&(1-w_j)\Big[-\frac{c}{B_0^2J}\left(I\frac{\partial\phi}{\partial\zeta}-g\frac{\partial\phi}{\partial\theta}\right)\frac{1}{f_{0j}}\left.\frac{\partial f_{0j}}{\partial\psi}\right|_{v_\perp}\\&-\frac{Z_j}{T_j}v_\parallel\frac{1}{B_0J}\left(\frac{\partial\phi}{\partial\theta}+q\frac{\partial\phi}{\partial\zeta}\right)\\&-\frac{1}{T_j}\frac{c}{B_0^2J}\left(\frac{m_jv_\parallel^2}{B_0}+\mu\right)\\&\times\left(g\frac{\partial B_0}{\partial\psi}\frac{\partial\phi}{\partial\theta}-I\frac{\partial B_0}{\partial\psi}\frac{\partial\phi}{\partial\zeta}-g\frac{\partial B_0}{\partial\theta}\frac{\partial\phi}{\partial\psi}\right)\\&+\frac{v_\parallel}{B_0J}\left(\frac{\partial\alpha}{\partial\zeta}I-\frac{\partial\alpha}{\partial\theta}g\right)\left(\frac{1}{f_{0j}}\left.\frac{\partial f_{0j}}{\partial\psi}\right|_{v_\perp}+\frac{Z_j}{T_j}\frac{\partial\phi}{\partial\psi}\right)\Big].\end{aligned} \tag{27}$$

3 Simulation results

In this section, we first use the contour plot of helical flux to show the island structures. We then show that ion and electron density profiles are partially flattened across the islands. The density profile of electrons is more flattened than that of ions, because electron orbits have a smaller radial width and are closer to the perturbed field lines. Since the trapped particles cannot move from one side of the island to the other side, they prevent the density profile to be totally flattened inside the islands. When the fraction of trapped particles decreases, the density profile becomes more flattened.

We choose m=2, n=1 islands and define the island perturbed vector potential as $A_{\rm I\parallel}=-0.0001R_0B_0\cos\left(2\theta-\zeta\right)$ in the simulation. The inverse aspect ratio is $a/R_0=0.42$. The island width is $0.16a$. Fig. 1 is the contour plot of the helical flux

for the islands at $\zeta = 0, \frac{\pi}{2}, \pi, \frac{3\pi}{2}$. We can see that the islands rotate in the toroidal direction, i.e., the poloidal position of the island center changes differently at different toroidal angles. The islands therefore break the toroidal symmetry and induce the mode coupling for toroidal drift-wave modes.

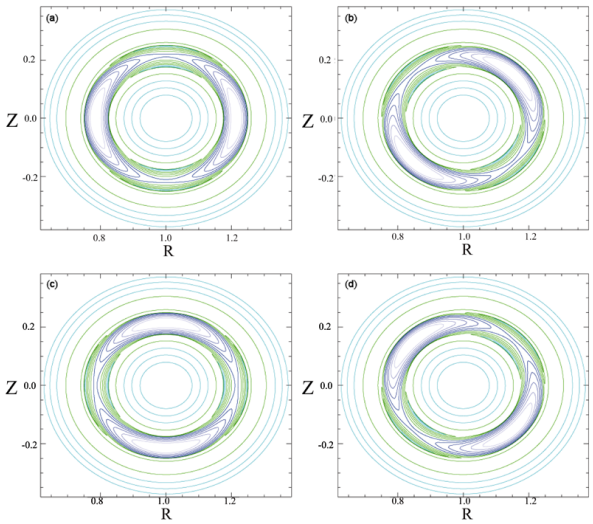

Fig.1 Helical flux surfaces of (2, 1) islands in the poloidal planes with the toroidal angle $\zeta = 0, \frac{\pi}{2}, \pi, \frac{3\pi}{2}$ (panel a, b, c, d, respectively)

We first investigate the ion density flattening across the islands, assuming uniform temperature. The initial ion density gradient at the center of the islands is $R_0/L_{ni} = 1.9$, where $L_{ni} = n_i\,(\mathrm{d}r/\mathrm{d}n_i)$ is the ion density scale length. Since the island width is much larger than the ion gyroradius, $W = 24\rho_i$, the ion finite-Lamor-radius (FLR) is not important. In the simulation, we do not include the self-consistent electric field or ion collisions. We exclude the electric field of the turbulence in this paper to illustrate the effects of the island on the density profiles in the absence of drift wave instabilities. GTC simulation with self-consistent electric field for the drift wave instabilities in the presence of magnetic islands has been published [14]. The only perturbation to the ion density profiles is the island perturbation. Since the ion should move along the field lines inside the islands, the density profile should be flattened. As shown in Fig. 2, at the island center on the high-field side, the ion density gradient decreases to zero after several ions transit times. After that, the value of ion density gradient oscillate up and down around zero because there is no collision to relax the system to a steady state. The time average of R_0/L_{ni} from $150R_0/c_s$ to $250R_0/c_s$ is 0.11, which shows that the ion density profile at the island center on the high-field side is almost flattened.

As shown in Fig. 3, the ion density profile at the low field side is less flattened than that at the high field side. The vertical lines are the island boundaries at $\theta = 0, \pi$. The toroidally trapped ions are mostly at the low field side. Compared with the motion of passing ions, the bounce motion of trapped ions can hardly be affected by the island perturbation. Since the trapped ions do not move across the islands, the ion density profile cannot be totally flattened at the low field side.

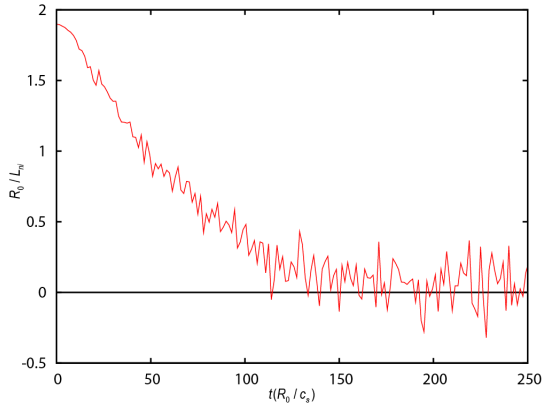

Fig.2 Time history of ion density gradient at the island center on the high field side

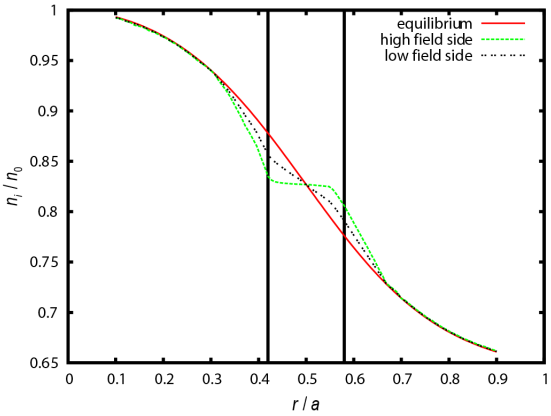

Fig.3 The equilibrium ion density profile at $\theta = 0, \pi$ (red solid line), the ion density profile at the high field side (green dotted line) and the ion density profile at the low field side (black dashed line)

For the electrons, we perform the simulation until the electron density gradient at the island center becomes zero. Then we plot electron density profiles at $\theta = 0, \pi$. In Fig. 4, the electron density profile at the low field side is also less flattened than that at the high field side due to the trapped electrons in the low field side. However, comparing with the ion density profile at the low field side, the electron density profile at the low field side is more flattened. Because the orbit widths of the trapped electrons are much smaller than those of ions, the trapped electrons can be affected more significantly by the islands than the ions.

In order to clarify the relation between the trapped particles and the density profile flattening, we investigate the radial profiles of ion density on the low field side for different trapped fractions. We change the inverse aspect ratios to get different trapped fractions η. When the inverse aspect ratios equal 0.42, 0.29 and 0.20, the corresponding trapped fractions are 0.48, 0.40 and 0.32, respectively. In Fig. 5, when the trapped fraction decreases, the ion density profiles become more

flattened because there are more passing ions which can move across the islands.

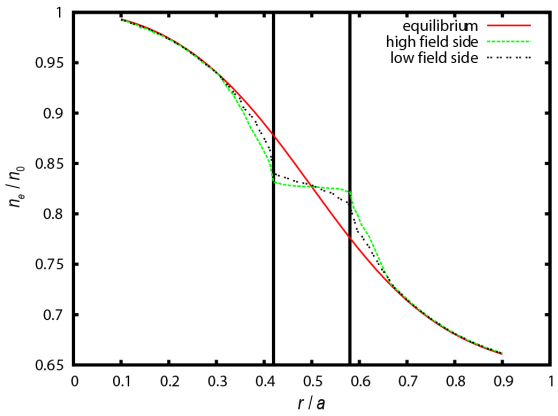

Fig.4 The equilibrium electron density profile at $\theta = 0, \pi$ (red solid line), the electron density profile at the high field side (green dotted line) and the electron density profile at the low field side (black dashed line)

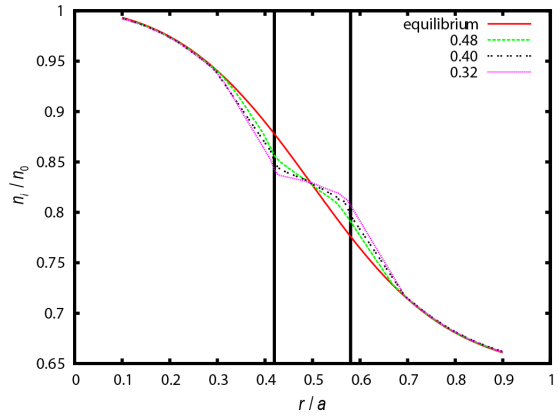

Fig.5 Ion density at the low field side ($\theta = 0$) with different trapped fractions ($\eta = 0.48, 0.40, 0.32$). The red solid line is the equilibrium ion density profile

4 Conclusions

We have implemented magnetic islands in the GTC and studied the flattening of the density profile inside the islands. The ion and electron density profiles become partially flattened inside the islands. The density profile at the low field side is less flattened than that at the high field side due to the toroidally trapped particles. When the fraction of trapped particles decreases, the density profile at the low field becomes more flattened since there are more particles moving along the perturbed field lines.

Acknowledgments

We are grateful for the discussions with and the support of the GTC team. This research used resources of the Oak Ridge Leadership Computing Facility at the Oak Ridge National Laboratory (DOE Contract No. DE-AC05-00OR22725), and the National Energy Research Scientific Computing Center (DOE Contract No. DE-AC02-05CH11231).

References

1 La Haye R J. 2006, Phys. Plasmas, 13: 055501
2 Chang Z, Callen J D, Fredrickson E D, et al. 1995, Phys. Rev. Lett., 74: 4663
3 Hender T C, Wesley J C, Bialek J, et al. 2007, Nucl. Fusion, 47: S128
4 Wilson H R, Connor J W, Hastie R J, et al. 1996, Phys. Plasmas, 3: 248
5 Rutherford P H. 1973, Phys. Fluids, 16: 1903
6 Connor J W, Waelbroeck F L, Wilson H R. 2001, Phys. Plasmas, 8: 2835
7 Rastovic D. 2015, Journal of Fusion Energy, 34: 207
8 Poli E, Bottino A, Peeters A G. 2009, Nucl. Fusion, 49: 075010
9 Poli E, Bottino A, Hornsby W A, et al. 2010, Plasma Phys. Control. Fusion, 52: 124021
10 Hornsby W A, Peeters A G, Snodin A P, et al. 2010, Phys. Plasmas, 17: 092301
11 Waltz R E, Waelbroeck F L. 2012, Phys. Plasmas, 19: 032508
12 Li J, Kishimoto Y. 2012, Phys. Plasmas, 19: 030705
13 Hornsby W A, Siccinio M, Peeters A G, et al. 2011, Plasma Phys. Control. Fusion, 53: 054008
14 Jiang P, Lin Z, Holod I, et al. 2014, Phys. Plasmas, 21: 122513
15 Lin Z, Hahm T S, Lee W W, et al. 1998, Science, 281: 1835
16 Holod I, Zhang W L, Xiao Y, et al. 2009, Phys. Plasmas, 16: 122307
17 Deng W, Lin Z, Holod I. 2012, Nucl. Fusion, 52: 023005
18 Lin Z, Tang W M, Lee W W. 1997, Phys. Rev. Lett., 78: 456
19 Zhang W, Lin Z, Chen L. 2008, Phys. Rev. Lett., 101: 095001
20 Lin Z, Holod I, Chen L. 2007, Phys. Rev. Lett., 99: 265003
21 Lin Z, Ethier S, Hahm T S, et al. 2012, Plasma Sci. Technol., 14: 1125
22 Xiao Y, Lin Z. 2009, Phys. Rev. Lett., 103: 085004
23 Zhang H S, Lin Z, Holod I. 2012, Phys. Rev. Lett., 109: 025001
24 Wang Z, Lin Z, Holod I, et al. 2013, Phys. Rev. Lett., 111: 145003
25 McClenaghan J, Lin Z, Holod I, et al. 2014, Phys. Plasmas, 21: 122519
26 Liu D, Zhang W, McClenaghan J, et al. 2014, Phys. Plasmas, 21: 122520
27 White R B, Chance M S. 1984, Physics of Fluids, 27: 2455
28 Carrera R, Hazeltine R D, Kotschenreuther M. 1986, Physics of Fluids, 29: 899

(Manuscript received 20 April 2015)
(Manuscript accepted 18 June 2015)
E-mail address of JIANG Peng: jiangp@pku.edu.cn